EUROPEAN LABORATORY FOR PARTICLE PHYSICS

CERN-PPE/97-109
11 August 1997

Multi-photon final states in e^+e^- collisions at $\sqrt{s} = 130 - 172$ GeV

The OPAL Collaboration

Abstract

The process $e^+e^- \to \gamma\gamma(\gamma)$ is studied using data recorded with the OPAL detector at LEP. The data sample corresponds to a total integrated luminosity of 25.38 pb^{-1} taken at centre-of-mass energies of 130 - 172 GeV. The measured cross-sections agree well with the expectation from QED. In a combined fit using data from all centre-of-mass energies, the angular distribution is used to obtain improved limits on the cut-off parameters: $\Lambda_+ > 195$ GeV and $\Lambda_- > 210$ GeV (95% CL). In addition, limits on non-standard $e^+e^-\gamma$ couplings and contact interactions, as well as a 95% CL mass limit for an excited electron, $M_{e^*} > 194$ GeV for an $e^+e^-\gamma$ coupling $\kappa = 1$, are determined.

(Submitted to Zeit. Phys. C)

The OPAL Collaboration

K. Ackerstaff[8], G. Alexander[23], J. Allison[16], N. Altekamp[5], K.J. Anderson[9], S. Anderson[12], S. Arcelli[2], S. Asai[24], D. Axen[29], G. Azuelos[18,a], A.H. Ball[17], E. Barberio[8], R.J. Barlow[16], R. Bartoldus[3], J.R. Batley[5], S. Baumann[3], J. Bechtluft[14], C. Beeston[16], T. Behnke[8], A.N. Bell[1], K.W. Bell[20], G. Bella[23], S. Bentvelsen[8], S. Bethke[14], O. Biebel[14], A. Biguzzi[5], S.D. Bird[16], V. Blobel[27], I.J. Bloodworth[1], J.E. Bloomer[1], M. Bobinski[10], P. Bock[11], D. Bonacorsi[2], M. Boutemeur[34], B.T. Bouwens[12], S. Braibant[12], L. Brigliadori[2], R.M. Brown[20], H.J. Burckhart[8], C. Burgard[8], R. Bürgin[10], P. Capiluppi[2], R.K. Carnegie[6], A.A. Carter[13], J.R. Carter[5], C.Y. Chang[17], D.G. Charlton[1,b], D. Chrisman[4], P.E.L. Clarke[15], I. Cohen[23], J.E. Conboy[15], O.C. Cooke[8], M. Cuffiani[2], S. Dado[22], C. Dallapiccola[17], G.M. Dallavalle[2], R. Davis[30], S. De Jong[12], L.A. del Pozo[4], K. Desch[3], B. Dienes[33,d], M.S. Dixit[7], E. do Couto e Silva[12], M. Doucet[18], E. Duchovni[26], G. Duckeck[34], I.P. Duerdoth[16], D. Eatough[16], J.E.G. Edwards[16], P.G. Estabrooks[6], H.G. Evans[9], M. Evans[13], F. Fabbri[2], M. Fanti[2], A.A. Faust[30], F. Fiedler[27], M. Fierro[2], H.M. Fischer[3], I. Fleck[8], R. Folman[26], D.G. Fong[17], M. Foucher[17], A. Fürtjes[8], D.I. Futyan[16], P. Gagnon[7], J.W. Gary[4], J. Gascon[18], S.M. Gascon-Shotkin[17], N.I. Geddes[20], C. Geich-Gimbel[3], T. Geralis[20], G. Giacomelli[2], P. Giacomelli[4], R. Giacomelli[2], V. Gibson[5], W.R. Gibson[13], D.M. Gingrich[30,a], D. Glenzinski[9], J. Goldberg[22], M.J. Goodrick[5], W. Gorn[4], C. Grandi[2], E. Gross[26], J. Grunhaus[23], M. Gruwé[8], C. Hajdu[32], G.G. Hanson[12], M. Hansroul[8], M. Hapke[13], C.K. Hargrove[7], P.A. Hart[9], C. Hartmann[3], M. Hauschild[8], C.M. Hawkes[5], R. Hawkings[27], R.J. Hemingway[6], M. Herndon[17], G. Herten[10], R.D. Heuer[8], M.D. Hildreth[8], J.C. Hill[5], S.J. Hillier[1], P.R. Hobson[25], R.J. Homer[1], A.K. Honma[28,a], D. Horváth[32,c], K.R. Hossain[30], R. Howard[29], P. Hüntemeyer[27], D.E. Hutchcroft[5], P. Igo-Kemenes[11], D.C. Imrie[25], M.R. Ingram[16], K. Ishii[24], A. Jawahery[17], P.W. Jeffreys[20], H. Jeremie[18], M. Jimack[1], A. Joly[18], C.R. Jones[5], G. Jones[16], M. Jones[6], U. Jost[11], P. Jovanovic[1], T.R. Junk[8], D. Karlen[6], V. Kartvelishvili[16], K. Kawagoe[24], T. Kawamoto[24], P.I. Kayal[30], R.K. Keeler[28], R.G. Kellogg[17], B.W. Kennedy[20], J. Kirk[29], A. Klier[26], S. Kluth[8], T. Kobayashi[24], M. Kobel[10], D.S. Koetke[6], T.P. Kokott[3], M. Kolrep[10], S. Komamiya[24], T. Kress[11], P. Krieger[6], J. von Krogh[11], P. Kyberd[13], G.D. Lafferty[16], R. Lahmann[17], W.P. Lai[19], D. Lanske[14], J. Lauber[15], S.R. Lautenschlager[31], J.G. Layter[4], D. Lazic[22], A.M. Lee[31], E. Lefebvre[18], D. Lellouch[26], J. Letts[12], L. Levinson[26], S.L. Lloyd[13], F.K. Loebinger[16], G.D. Long[28], M.J. Losty[7], J. Ludwig[10], A. Macchiolo[2], A. Macpherson[30], M. Mannelli[8], S. Marcellini[2], C. Markus[3], A.J. Martin[13], J.P. Martin[18], G. Martinez[17], T. Mashimo[24], P. Mättig[3], W.J. McDonald[30], J. McKenna[29], E.A. Mckigney[15], T.J. McMahon[1], R.A. McPherson[8], F. Meijers[8], S. Menke[3], F.S. Merritt[9], H. Mes[7], J. Meyer[27], A. Michelini[2], G. Mikenberg[26], D.J. Miller[15], A. Mincer[22,e], R. Mir[26], W. Mohr[10], A. Montanari[2], T. Mori[24], M. Morii[24], U. Müller[3], S. Mihara[24], K. Nagai[26], I. Nakamura[24], H.A. Neal[8], B. Nellen[3], R. Nisius[8], S.W. O'Neale[1], F.G. Oakham[7], F. Odorici[2], H.O. Ogren[12], A. Oh[27], N.J. Oldershaw[16], M.J. Oreglia[9], S. Orito[24], J. Pálinkás[33,d], G. Pásztor[32], J.R. Pater[16], G.N. Patrick[20], J. Patt[10], M.J. Pearce[1], R. Perez-Ochoa[8], S. Petzold[27], P. Pfeifenschneider[14], J.E. Pilcher[9], J. Pinfold[30], D.E. Plane[8], P. Poffenberger[28], B. Poli[2], A. Posthaus[3], D.L. Rees[1], D. Rigby[1], S. Robertson[28], S.A. Robins[22], N. Rodning[30], J.M. Roney[28], A. Rooke[15], E. Ros[8], A.M. Rossi[2], P. Routenburg[30], Y. Rozen[22], K. Runge[10], O. Runolfsson[8], U. Ruppel[14], D.R. Rust[12], R. Rylko[25], K. Sachs[10], T. Saeki[24], E.K.G. Sarkisyan[23], C. Sbarra[29], A.D. Schaile[34], O. Schaile[34], F. Scharf[3], P. Scharff-Hansen[8], P. Schenk[34], J. Schieck[11], P. Schleper[11],

B. Schmitt[8], S. Schmitt[11], A. Schöning[8], M. Schröder[8], H.C. Schultz-Coulon[10], M. Schumacher[3], C. Schwick[8], W.G. Scott[20], T.G. Shears[16], B.C. Shen[4], C.H. Shepherd-Themistocleous[8], P. Sherwood[15], G.P. Siroli[2], A. Sittler[27], A. Skillman[15], A. Skuja[17], A.M. Smith[8], G.A. Snow[17], R. Sobie[28], S. Söldner-Rembold[10], R.W. Springer[30], M. Sproston[20], K. Stephens[16], J. Steuerer[27], B. Stockhausen[3], K. Stoll[10], D. Strom[19], P. Szymanski[20], R. Tafirout[18], S.D. Talbot[1], S. Tanaka[24], P. Taras[18], S. Tarem[22], R. Teuscher[8], M. Thiergen[10], M.A. Thomson[8], E. von Törne[3], S. Towers[6], I. Trigger[18], Z. Trócsányi[33], E. Tsur[23], A.S. Turcot[9], M.F. Turner-Watson[8], P. Utzat[11], R. Van Kooten[12], M. Verzocchi[10], P. Vikas[18], E.H. Vokurka[16], H. Voss[3], F. Wäckerle[10], A. Wagner[27], C.P. Ward[5], D.R. Ward[5], P.M. Watkins[1], A.T. Watson[1], N.K. Watson[1], P.S. Wells[8], N. Wermes[3], J.S. White[28], B. Wilkens[10], G.W. Wilson[27], J.A. Wilson[1], G. Wolf[26], T.R. Wyatt[16], S. Yamashita[24], G. Yekutieli[26], V. Zacek[18], D. Zer-Zion[8]

[1]School of Physics and Space Research, University of Birmingham, Birmingham B15 2TT, UK
[2]Dipartimento di Fisica dell' Università di Bologna and INFN, I-40126 Bologna, Italy
[3]Physikalisches Institut, Universität Bonn, D-53115 Bonn, Germany
[4]Department of Physics, University of California, Riverside CA 92521, USA
[5]Cavendish Laboratory, Cambridge CB3 0HE, UK
[6] Ottawa-Carleton Institute for Physics, Department of Physics, Carleton University, Ottawa, Ontario K1S 5B6, Canada
[7]Centre for Research in Particle Physics, Carleton University, Ottawa, Ontario K1S 5B6, Canada
[8]CERN, European Organisation for Particle Physics, CH-1211 Geneva 23, Switzerland
[9]Enrico Fermi Institute and Department of Physics, University of Chicago, Chicago IL 60637, USA
[10]Fakultät für Physik, Albert Ludwigs Universität, D-79104 Freiburg, Germany
[11]Physikalisches Institut, Universität Heidelberg, D-69120 Heidelberg, Germany
[12]Indiana University, Department of Physics, Swain Hall West 117, Bloomington IN 47405, USA
[13]Queen Mary and Westfield College, University of London, London E1 4NS, UK
[14]Technische Hochschule Aachen, III Physikalisches Institut, Sommerfeldstrasse 26-28, D-52056 Aachen, Germany
[15]University College London, London WC1E 6BT, UK
[16]Department of Physics, Schuster Laboratory, The University, Manchester M13 9PL, UK
[17]Department of Physics, University of Maryland, College Park, MD 20742, USA
[18]Laboratoire de Physique Nucléaire, Université de Montréal, Montréal, Quebec H3C 3J7, Canada
[19]University of Oregon, Department of Physics, Eugene OR 97403, USA
[20]Rutherford Appleton Laboratory, Chilton, Didcot, Oxfordshire OX11 0QX, UK
[22]Department of Physics, Technion-Israel Institute of Technology, Haifa 32000, Israel
[23]Department of Physics and Astronomy, Tel Aviv University, Tel Aviv 69978, Israel
[24]International Centre for Elementary Particle Physics and Department of Physics, University of Tokyo, Tokyo 113, and Kobe University, Kobe 657, Japan
[25]Brunel University, Uxbridge, Middlesex UB8 3PH, UK
[26]Particle Physics Department, Weizmann Institute of Science, Rehovot 76100, Israel
[27]Universität Hamburg/DESY, II Institut für Experimental Physik, Notkestrasse 85, D-22607

Hamburg, Germany
[28]University of Victoria, Department of Physics, P O Box 3055, Victoria BC V8W 3P6, Canada
[29]University of British Columbia, Department of Physics, Vancouver BC V6T 1Z1, Canada
[30]University of Alberta, Department of Physics, Edmonton AB T6G 2J1, Canada
[31]Duke University, Dept of Physics, Durham, NC 27708-0305, USA
[32]Research Institute for Particle and Nuclear Physics, H-1525 Budapest, P O Box 49, Hungary
[33]Institute of Nuclear Research, H-4001 Debrecen, P O Box 51, Hungary
[34]Ludwigs-Maximilians-Universität München, Sektion Physik, Am Coulombwall 1, D-85748 Garching, Germany

[a] and at TRIUMF, Vancouver, Canada V6T 2A3
[b] and Royal Society University Research Fellow
[c] and Institute of Nuclear Research, Debrecen, Hungary
[d] and Department of Experimental Physics, Lajos Kossuth University, Debrecen, Hungary
[e] and Department of Physics, New York University, NY 1003, USA

1 Introduction

This paper reports a study of the annihilation process $e^+e^- \to \gamma\gamma(\gamma)$ using data recorded with the OPAL detector at LEP. At LEP energies, this is one of the few processes having negligible contributions from the weak interaction. Since the QED differential cross-section is precisely predicted in theory, deviations from the expected angular distribution are a sensitive test for non-standard physics processes contributing to these photonic final states.

The OPAL collaboration has previously published a study of photonic final states, with and without missing energy, at $\sqrt{s}$ = 130 - 140 GeV [1]. The present analysis concentrates on final states with two or more detected photons, but no missing transverse momentum, to study only the QED process. Photonic final states with missing energy have been analysed separately [2].

Any non-QED effects described by the general framework of effective Lagrangian theory should increase with centre-of-mass energy. Existing OPAL limits on deviations from QED can be improved by using the data at centre-of-mass energies of 161.3 GeV and 172.1 GeV. A small amount of data taken at 170.3 GeV is included in the 172 GeV sample. The corresponding integrated luminosities of these data sets are 9.97 and 10.13 pb^{-1}, respectively. Since the selection criteria have changed, previously analysed data taken at centre-of-mass energies of 130.3 GeV (2.69 pb^{-1}) and 136.2 GeV (2.59 pb^{-1}) are reanalysed here to allow for a coherent treatment. The 136 GeV sample includes a small amount of data taken at 140.2 GeV. The error on the luminosity differs slightly for the different energies and is approximately 0.5% .

These measurements test QED at the highest centre-of-mass energies. Possible deviations are conveniently parametrised by cut-off parameters $\Lambda_\pm$. A comparison of the measured photon angular distribution with the QED expectation leads to limits on the QED cut-off parameters $\Lambda_\pm$, contact interactions ($e^+e^-\gamma\gamma$) and non-standard $e^+e^-\gamma$-couplings as described in section 3.

The possible effects of an excited electron, e^*, which would also change the angular distribution, are investigated. In addition, the possible production of a resonance X via $e^+e^- \to X\gamma$, followed by the decay $X \to \gamma\gamma$, is studied in the invariant mass spectrum of photon pairs in three-photon final states.

The following section contains a brief description of the OPAL detector and the Monte Carlo simulated event samples. Section 3 describes the QED differential cross-sections for $e^+e^- \to \gamma\gamma(\gamma)$, as well as those from several models containing extensions to QED. In sections 4 - 6 the analysis is described in detail. The results are presented in section 7.

2 The OPAL detector and Monte Carlo samples

A detailed description of the OPAL detector can be found in [3]. OPAL uses a right-handed coordinate system in which the z axis is along the electron beam direction and the x axis is horizontal. The polar angle, θ, is measured with respect to the z axis and the azimuthal angle, ϕ, with respect to the x axis. For this analysis the most important detector component is the electromagnetic calorimeter (ECAL) which is divided into two parts, the barrel and the endcaps. The barrel covers the polar angle range of $|\cos\theta| < 0.81$ and consists of 9440 lead-glass blocks. The endcaps cover the polar angle range of $0.81 < |\cos\theta| < 0.98$ and consist of 1132 blocks. In this analysis, the central tracking detector is used primarily to reject events inconsistent with purely photonic final states. Raw hit information from the vertex drift chamber (CV) and jet drift chamber (CJ) is used to reject events with tracks coming from the interaction point. CV is divided into 36 ϕ-sectors and its inner 12 (6) axial layers cover an angular range of $|\cos\theta| < 0.95(0.97)$. CJ is divided into 24 ϕ-sectors and covers an angular range of $|\cos\theta| < 0.97$ with its inner 16 layers. Incorporated in the surrounding magnet yoke is the hadronic calorimeter (HCAL) covering 97% of the solid angle. The outermost detectors are the muon chambers, shielded from the interaction point by at least 1.3 m of iron and covering the polar angle range of $|\cos\theta| < 0.985$.

Different Monte Carlo samples are used to study efficiency and background. For the signal process $e^+e^- \to \gamma\gamma(\gamma)$ the RADCOR [4] generator is used. It provides a $\mathcal{O}(\alpha^3)$ cross section up to $|\cos\theta| = 1$ for the photon angle. No Monte Carlo with complete fourth order is currently available. The only program that generates four-photon final states neglects the mass of the electron and therefore does not correctly include photons in the far forward range. The Bhabha process is studied with two different programs. BHWIDE [5] generates both electron and positron in the acceptance of the detector. In contrast, TEEGG [6] allows one of them to have very low energy or escape along the beam-pipe, in addition, one photon is scattered into the detector. The process $e^+e^- \to \overline{\nu}\nu\gamma(\gamma)$ is studied with NUNUGPV [7]. Both $e^+e^- \to \mu^+\mu^-$ and $e^+e^- \to \tau^+\tau^-$ are simulated using KORALZ [8] and PYTHIA [9] is used for hadronic events. All samples were processed through the OPAL detector simulation program [10] and reconstructed as for real data.

3 Cross section for the process $e^+e^- \to \gamma\gamma$

The differential cross-section for the process $e^+e^- \to \gamma\gamma$ in the relativistic limit of lowest order QED is given by [11]:

$$\left(\frac{d\sigma}{d\Omega}\right)_{\rm Born} = \frac{\alpha^2}{s}\,\frac{1+\cos^2\theta}{1-\cos^2\theta}. \tag{1}$$

where s denotes the square of the centre-of-mass energy, α is the electromagnetic coupling constant and θ the polar angle of one photon. Since the two photons cannot be distinguished the event angle is defined such that $\cos\theta$ is positive.

In Ref. [12] possible deviations from the QED cross-section for Bhabha and Møller scattering are parametrized in terms of cut-off parameters. These parameters correspond to a short range exponential term added to the Coulomb potential. This ansatz leads to a modification of the photon angular distribution as given in Eq. (2).

$$\left(\frac{d\sigma}{d\Omega}\right)_{\Lambda_\pm} = \left(\frac{d\sigma}{d\Omega}\right)_{\rm Born}\left[1 \pm \frac{s^2}{2\Lambda_\pm^4}\sin^2\theta\right] \tag{2}$$

Alternatively, in terms of effective Lagrangian theory, a gauge invariant operator may be added to QED. Depending on the dimension of the operator different deviations from QED can be formulated [13]. Contact interactions ($\gamma\gamma e^+e^-$) or non-standard γe^+e^- couplings described by dimension 6, 7 or 8 operators lead to angular distributions with different mass scales Λ (see Eqs. 3 - 5). The subscripts (QED+6 etc.) follow the notation in Ref. [13].

$$\left(\frac{d\sigma}{d\Omega}\right)_{\rm QED+6} = \left(\frac{d\sigma}{d\Omega}\right)_{\rm Born}\left[1 + \frac{s^2}{\alpha\Lambda_6^4}\sin^2\theta\right] \tag{3}$$

$$\left(\frac{d\sigma}{d\Omega}\right)_{\rm QED+7} = \left(\frac{d\sigma}{d\Omega}\right)_{\rm Born} + \frac{s^2}{32\pi}\frac{1}{\Lambda_7^6} \tag{4}$$

$$\left(\frac{d\sigma}{d\Omega}\right)_{\rm QED+8} = \left(\frac{d\sigma}{d\Omega}\right)_{\rm Born} + \frac{s^2 m_{\rm e}^2}{32\pi}\frac{1}{\Lambda_8^8} \tag{5}$$

The definition of Eq. (3) is identical to the standard definition (Eq. 2) if $\Lambda_\pm^4 = \frac{\alpha}{2}\Lambda_6^4$. Similarly Eq. (4) is equivalent to Eq. (5) if $\Lambda_8^8 = m_{\rm e}^2\,\Lambda_7^6$. Therefore only the parameters of Eq. (2) and (4) are determined by a fit to obtain limits on deviations from QED. The limits on the other parameters can easily be derived from these results.

The existence of an excited electron e^* with an $e^*e\gamma$ coupling would contribute to the photon production process via t-channel exchange. The resulting deviation from $\left(\frac{d\sigma}{d\Omega}\right)_{\rm Born}$ depends on the e^* mass M_{e^*} and the coupling constant κ of the $e^*e\gamma$ vertex [14]:

$$\begin{aligned}\left(\frac{d\sigma}{d\Omega}\right)_{e^*} &= \left(\frac{d\sigma}{d\Omega}\right)_{\rm Born} + \\ \alpha^2\Bigg\{ &\frac{1}{2}\left(\frac{\kappa}{M_{e^*}}\right)^4\left(E^2\sin^2\theta + M_{e^*}^2\right)\left(\frac{q^4}{(q^2-M_{e^*}^2)^2} + \frac{q'^4}{(q'^2-M_{e^*}^2)^2}\right) \\ &+ 4\left(\frac{\kappa}{M_{e^*}}\right)^4\frac{M_{e^*}^2\,E^4\,\sin^2\theta}{(q^2-M_{e^*}^2)(q'^2-M_{e^*}^2)} \\ &+ \left(\frac{\kappa}{M_{e^*}}\right)^2\left[\frac{q^2}{q^2-M_{e^*}^2} + \frac{q'^2}{q'^2-M_{e^*}^2} + E^2\sin^2\theta\left(\frac{1}{q^2-M_{e^*}^2} + \frac{1}{q'^2-M_{e^*}^2}\right)\right]\Bigg\},\end{aligned} \tag{6}$$

with the beam energy $E = \sqrt{s}/2$, $q^2 = -2E^2(1-\cos\theta)$ and $q'^2 = -2E^2(1+\cos\theta)$. In the limit $M_{e^*} \gg \sqrt{s}$, the mass is related to the cut-off parameter by $M_{e^*} = \sqrt{\kappa}\,\Lambda_+$.

4 Event angle definition and radiative corrections

For the process $e^+e^- \to \gamma_1\gamma_2$ the polar angle θ of the event is defined by the angle between either of the two photons and the beam direction since $|\cos\theta_1| = |\cos\theta_2|$. This is a good approximation for most of the events under consideration, since additional photons tend to be soft. For many events, however, there is a third energetic photon and thus $|\cos\theta_1| \neq |\cos\theta_2|$ in general. Several angle definitions are possible to characterize an event. The following two are considered:

$$\cos\theta_{\rm av} = \frac{|\cos\theta_1| + |\cos\theta_2|}{2}, \tag{7}$$

$$\cos\theta^* = \left|\sin\frac{\theta_1-\theta_2}{2}\right| \Big/ \sin\frac{\theta_1+\theta_2}{2}, \tag{8}$$

where θ_1 and θ_2 are the polar angles of the most energetic photons. Both $\cos\theta_{\rm av}$ and $\cos\theta^*$ are identical to $|\cos\theta|$ for two-photon final states. For three-photon events in which the third photon is along the beam direction, θ^* is equivalent to the scattering angle in the centre-of-mass system of the two observed photons.

Fig. 1 shows the ratio of the angular distributions using both $\cos\theta_{\rm av}$ and $\cos\theta^*$, relative to the Born cross section as derived using an $\mathcal{O}(\alpha^3)$ $e^+e^- \to \gamma\gamma(\gamma)$ Monte Carlo generator [4]. The event angles are calculated from the two photons with the highest generated energy. The comparison is made at the generator level, i.e. without detector simulation and efficiency effects. It can be seen that the distribution of $\cos\theta_{\rm av}$ (Eq. 7) shows large deviations from the lowest order (Born) distribution for much of the $\cos\theta$ range. For this analysis $\cos\theta^*$ (Eq. (8)) is chosen because it better matches the shape of the Born distribution over the range $\cos\theta^* < 0.9$ considered in this analysis.

5 Event selection

Events are selected by requiring two or more clusters in the electromagnetic calorimeter (ECAL). A cluster is selected as a photon candidate if it is within the polar angle range $|\cos\theta| < 0.97$. The cluster must consist of at least two lead-glass blocks, with a combined ECAL energy deposit exceeding 1 GeV uncorrected for possible energy loss in the material before the ECAL. Events with a photon candidate having five or more reconstructed clusters within a cone with a half-angle of 11.5° are rejected. This isolation criterion helps to reduce some instrumental background.

There are two major classes of background remaining to the $\gamma\gamma(\gamma)$ signature. The first can be identified by the presence of primary charged tracks. Bhabha events, for example, have similar electromagnetic cluster characteristics as $\gamma\gamma(\gamma)$ events, but are normally easily distinguished

by the presence of charged tracks. The second class consists of events without primary charged tracks. Certain cosmic ray events and the Standard Model process $e^+e^- \to \bar{\nu}\nu\gamma\gamma$ contribute to this background.

5.1 Neutral events

Events having only photons in the final state are classified as 'neutral events'. They should not have any charged track consistent with coming from the interaction point. The rejection of all events having tracks in the central tracking chambers CV or CJ would lead to an efficiency loss because of converted photons. Nevertheless, contributions from any channel with primary charged tracks should be reduced to a negligible level.

To reject events with primary charged tracks while retaining efficiency for converted photons, only the inner part of the drift chambers are considered. First, the correlation between the observed clusters and charged hit activity in both drift chambers is used. Hits are counted in the ϕ-sectors of CV and CJ which are geometrically associated to each cluster. A correlation is assigned to a cluster if there are more than a given number of wires with hits in the associated ϕ-sector.

- A CV correlation is assigned if there are at least m wires with hits in the n CV layers nearest to the beam-pipe (denoted by m/n), depending on $\cos\theta$ of the cluster:

Cut on m/n	$\cos\theta$ region		
6/12	0.	$< \lvert\cos\theta\rvert <$	0.75
5/8	0.75	$< \lvert\cos\theta\rvert <$	0.95
4/6 or 5/8	0.95	$< \lvert\cos\theta\rvert <$	0.97

- A CJ correlation is assigned if there are at least 12 wires with hits in the inner 16 CJ layers, independent of the cluster polar angle.

Two vetoes are defined using combinations of these hit activity correlations in CV and CJ. A third veto tests for reconstructed charged tracks not correlated with either of the clusters. Any of the three vetoes rejects the event.

- The **single veto** requires that both the CV and CJ correlation are assigned for any cluster.
- The **double veto** requires that for each of the highest energy clusters either the CV or CJ correlation is assigned.
- The **unassociated track veto** requires that there be no reconstructed track with a transverse momentum of more than 1 GeV and at least 20 hits in CJ, separated by more than 10° in ϕ from all photon candidates.

5.2 Cosmic ray events

A cosmic ray particle can pass through the hadronic and electromagnetic calorimeters without necessarily producing a reconstructed track in the central tracking chambers. Events of this type are rejected if there are 3 or more hits in the muon chambers. In the case of 1 or 2 muon hits the event is rejected if the highest energy HCAL cluster with at least 1 GeV is separated from each of the photon candidates by more than 10° in ϕ. Events are rejected if the cluster extent in $\cos\theta$ is larger than 0.4. This cut is primarily to reject beam halo events.

5.3 Kinematic selection

The event sample is divided into three classes *I*, *II* and *III*. The classes are distinguished by the number of photon candidates and the acollinearity angle ζ, defined as $\zeta = 180^\circ - \xi$, where ξ is the angle between the two highest energy clusters. Different selections are applied to each class separately, to make use of the different kinematics. Only events with $\cos\theta^* < 0.9$ are selected to avoid systematic errors due to large efficiency and radiative corrections.

All events having an acollinearity angle $\zeta < 10^\circ$ (i.e. the two highest energy clusters are almost collinear) belong to class *I* independent of the number of photon candidates. For true $e^+e^- \to \gamma\gamma(\gamma)$ events in this class, the sum of the two highest cluster energies $E_S = E_1 + E_2$ should almost be equal to the centre-of-mass energy $\sqrt{s}$. The distribution of E_S is shown in Fig. 2. Events having $E_S > 0.6\sqrt{s}$ are selected. This cut is well below the tail of the energy distribution for $e^+e^- \to \gamma\gamma(\gamma)$ Monte Carlo events as shown in the figure.

Class *II* contains acollinear events ($\zeta > 10^\circ$) with exactly two observed photon candidates. Events of this class typically contain an energetic photon that escapes detection near the beam-pipe ($|\cos\theta| > 0.97$). If the polar angle of this photon is approximated as $|\cos\theta| = 1$, its energy, $E_{\rm lost}$ (Eq. 9), can be estimated from the angles of the observed photons θ_1 and θ_2. The energy sum E_S is then defined as the sum of the two observed cluster energies and the lost energy.

$$E_{\rm lost} = \sqrt{s}\left(1 + \frac{\sin\theta_1 + \sin\theta_2}{|\sin(\theta_1+\theta_2)|}\right)^{-1} \quad (9)$$

$$E_S = E_1 + E_2 + E_{\rm lost} \quad (10)$$

The imbalance $\mathcal{B}$, defined as

$$\mathcal{B} = (\sin\theta_1 + \sin\theta_2)\left|\cos\left(\frac{\phi_1 - \phi_2}{2}\right)\right|, \quad (11)$$

provides an approximate measure of the scaled transverse momentum of the event without using the cluster energies. Fig. 3 shows the distributions of $\mathcal{B}$ and E_S. It can be seen that the background (mainly $\nu\overline{\nu}\gamma\gamma$) is uniformly distributed in $\mathcal{B}$ whereas the signal is peaked at low values. Events are selected if $\mathcal{B} < 0.2$ and $E_S > 0.6\sqrt{s}$. Since the angular definition discussed in section 4 uses the two highest energy photons, events are rejected if $E_{\rm lost}$ exceeds the energy of either observed photon.

Class *III* contains acollinear events ($\zeta > 10^\circ$) having 3 or more observed photon candidates. To calculate the transverse and longitudinal momenta ($p_{\rm t}$, $p_{\rm l}$) of the system the cluster energies

have to be used in addition to the photon angles. Since a non-zero longitudinal momentum could correspond to an additional photon along the beam direction, the energy sum E_S is calculated as sum of the cluster energies E_i and p_l:

$$E_S = \sum_{i=1}^{n} E_i + p_\mathrm{l}. \tag{12}$$

Fig. 4 shows the distribution of $E_S/\sqrt{s}$ versus $p_\mathrm{t}/\sqrt{s}$ for $\mathrm{e^+e^-} \to \gamma\gamma(\gamma)$ Monte Carlo and for the data. In the data the $\mathrm{e^+e^-} \to \gamma\gamma(\gamma)$ events are clearly separated from the background by the fact that they have small transverse momenta and an energy sum around the centre-of-mass energy. The main part of the background originates from cosmic ray events without hits in the muon chambers. The selection requirements $E_S > 0.6\sqrt{s}$ and $p_\mathrm{t} < 0.1\sqrt{s}$ easily reject these events.

No event with more than three clusters is observed. The angle sum $\sum\alpha$ is used to identify planar three-photon events:

$$\sum\alpha = \alpha_{ij} + \alpha_{ik} + \alpha_{kj}, \tag{13}$$

with α_{ij} the angle between photons i and j. Seven planar events with $\sum\alpha > 350^\circ$ are accepted as three-photon events and included in the sample of $\mathrm{e^+e^-} \to \gamma\gamma(\gamma)$. Two other events are consistent with three detected photons and an additional photon along the beam direction.

The kinematic requirements used to select each of the event classes are summarised in Tab. 1.

Event class		Requirements
all		$\cos\theta^* < 0.9$
I		$\zeta < 10^\circ$
		$E_S > 0.6\sqrt{s}$
II		$\zeta > 10^\circ$
		$E_S > 0.6\sqrt{s}$
		$E_1, E_2 > E_\mathrm{lost}$
		$\mathcal{B} < 0.2$
		2 photon candidates
III		$\zeta > 10^\circ$
		$E_S > 0.6\sqrt{s}$
		$p_t < 0.1\sqrt{s}$
		≥ 3 photon candidates
	planar	$\sum\alpha > 350^\circ$
	nonplanar	$\sum\alpha < 350^\circ$

Table 1: Summary of the kinematic cuts. For definition of the variables see the text.

6 Corrections and systematic errors

Since the deviations from QED (Eqs. 2 - 6) are given with respect to Born level, the observed angular distributions need to be corrected to Born level. The effect of radiative corrections to the

Born level calculation is quantified by $\mathcal{R}$, the ratio of the angular distribution of $e^+e^- \to \gamma\gamma(\gamma)$ Monte Carlo and the Born cross-section as shown in Fig. 1:

$$\mathcal{R} = \left(\frac{d\sigma}{d\Omega}\right)_{\mathrm{MC}} (\cos\theta^*) \Bigg/ \left(\frac{d\sigma}{d\Omega}\right)_{\mathrm{Born}} . \tag{14}$$

The ratio $\mathcal{R}$ is used to correct the data bin by bin to the Born level. A 1% error on the total cross-section from higher order effects is assumed. No error on the slope of the distribution is included in the results. Since the $\mathcal{O}(\alpha^3)$ radiative corrections are small, the $\mathcal{O}(\alpha^4)$ effects are assumed to be negligible.

The efficiency and angular resolution of the reconstruction is determined using a Monte Carlo sample with full detector simulation. The efficiency is reasonably constant for $\cos\theta^* < 0.9$, but drops rapidly for $\cos\theta^* > 0.9$. The overall efficiency for $\cos\theta^* < 0.9$ is 91.9% with a maximum of 95% in the barrel of the detector. A polynomial parametrisation $\mathcal{E}(\cos\theta^*)$ is used for the efficiency correction. Due to uncertainties of the photon conversion probability and the Monte Carlo statistics a 1% systematic error is assumed for the efficiency. The agreement between generated and reconstructed angles is very good. An angular resolution of 0.3° full width at half maximum is obtained. Background is studied using Monte Carlo events from the processes shown in Tab. 2. The expected ratio of background to signal is less than 0.4% and is neglected.

Process Generator	Background events
$e^+e^- \to e^+e^-$ (BHWIDE)	< 0.24
$e^+e^- \to e^+e^-$ (TEEGG)	< 0.67
$e^+e^- \to \bar{\nu}\nu\gamma\gamma$	< 0.02
$e^+e^- \to \mu^+\mu^-$	< 0.04
$e^+e^- \to \tau^+\tau^-$	< 0.05
$e^+e^- \to \bar{q}q$	< 0.02

Table 2: Estimated 95 % CL upper limits for expected background processes from Monte Carlo at $\sqrt{s}$ = 130 - 172 GeV.

The probability that a signal event is rejected by the neutral event selection due to random instrumental background causing a veto is studied with randomly-triggered events. For the single veto the probability is 4×10^{-4} and it is 1×10^{-4} for both the double veto and the track veto for. The small overall veto probability of 5×10^{-4} is therefore neglected. The systematic errors on the total cross-section are summarized in Tab. 3.

	Uncertainty
Luminosity	0.5%
Radiative correction $\mathcal{R}$	1.0%
Selection efficiency $\mathcal{E}$	1.0%
Background	< 0.4%
Total	1.6%

Table 3: Summary of systematic errors on the cross-section

7 Results

In Tab. 4 the numbers of observed events in each class are compared to the QED expectations. The derived total cross-section σ in the range $\cos\theta^* < 0.9$ is plotted in Fig. 5 as a function of the centre-of-mass energy. The numerical results for the cross-section are given in Tab. 4. They are corrected for efficiency loss and $\mathcal{O}(\alpha^3)$ effects. All numbers agree well with QED expectations.

The measured differential cross-sections at 130, 136, 161 and 172 GeV centre-of-mass energies are shown in Figs. 6 and 7 together with a fit of the function $\left(\frac{d\sigma}{d\Omega}\right)_{\Lambda_\pm}$ (Eq. 2). The fit to the distribution is performed using the binned log likelihood method. The likelihood function $\mathcal{L}$ is based on Poisson statistics and defined as:

$$\mathcal{L}_i = \frac{\mu_i^{n_i}}{n_i!} e^{-\mu_i} \tag{15}$$

with n_i the number of observed and μ_i the number of expected events per $\cos\theta$ bin i. To determine μ_i the model dependent cross-section function $\frac{d\sigma}{d\Omega}$ is not integrated over the bin. Instead a simple procedure is applied in which the central value x_i of the bin is determined as defined in Ref. [15]:

$$\left(\frac{d\sigma}{d\Omega}\right)_{\text{Born}}(x_i) = \frac{1}{x_u - x_l} \int_{x_l}^{x_u} \left(\frac{d\sigma}{d\Omega}\right)_{\text{Born}}(y)dy, \tag{16}$$

where x_l and x_u are the lower and upper boundaries of the bin i. In this way the differential function $\frac{d\sigma}{d\Omega}$ can be directly compared to the integrated number of events presented as a histogram. The mean efficiency $\mathcal{E}_i$ and radiative corrections $\mathcal{R}_i$ are included in the expectation μ_i

Energy $\sqrt{s}$ [GeV]	130		136	
	Expected	Observed	Expected	Observed
Class *I*	34.3±0.9	33	30.1±0.8	26
Class *II*	4.0±0.3	2	3.5±0.3	3
Class *III* planar	1.0±0.2	2	0.9±0.2	0
Class *III* nonplanar	–	0	–	0
$\sigma_{\text{tot}}^{\text{Born}}$	15.7	14.9±2.5	14.3	12.2±2.2
Energy $\sqrt{s}$ [GeV]	161		172	
	Expected	Observed	Expected	Observed
Class *I*	85.8±0.6	90	77.6±0.7	75
Class *II*	9.0±0.2	8	8.0±0.2	14
Class *III* planar	1.9±0.1	3	1.8±0.1	2
Class *III* nonplanar	–	1	–	1
$\sigma_{\text{tot}}^{\text{Born}}$	10.2	10.9±1.1	9.0	9.7±1.0

Table 4: Comparison of number of observed events and Monte Carlo prediction. For nonplanar events no expectation is given, since the $\mathcal{O}(\alpha^3)$ Monte Carlo does not include these events. The two observed class *III* nonplanar events are kinematically compatible with a fourth photon along the beam-direction. In addition the total cross section corrected to the Born level is given.

for each bin. To allow the total number of expected events to vary within the systematic error, a normalization factor ϵ is added:

$$\mu_i = \epsilon \, \frac{d\sigma}{d\Omega}(x_i) \; (x_u - x_l) \mathcal{E}_i \mathcal{R}_i L \tag{17}$$

$$\mathcal{E}_i = \frac{1}{n_i} \sum_{j=1}^{n_i} \mathcal{E}(\cos\theta_j), \tag{18}$$

where L is the integrated luminosity and $\cos\theta_j$ is the angle of the j-th event. An estimator function P is defined which includes a Gaussian term with mean 1 and width $\delta = 0.016$ (see Tab. 3) to account for the error of the normalization ϵ. The routine MINOS [16], which provides asymmetric errors, is used to minimize P:

$$\begin{aligned} P &= \frac{(\epsilon - 1)^2}{\delta^2} + \sum_i -2 \; \ln \mathcal{L}_i \\ &= \frac{(\epsilon - 1)^2}{\delta^2} + \sum_i 2 \left(\mu_i - \; n_i \ln \mu_i \right). \end{aligned} \tag{19}$$

The fit is performed with two free parameters: the normalization ϵ and the model dependent parameter λ (see Tab. 5 and Eqs. 2, 4 and 6). To obtain the limits at 95% confidence level the probability is normalized to the physically allowed region, i.e. $\lambda_+ > 0$ and $\lambda_- < 0$ as described in Ref. [17].

Results for the different parameters are obtained from a simultaneous fit to the angular distibutions for each centre-of-mass energy. A fit is also performed for each centre-of-mass energy separately, with the results for $\Lambda_\pm$ given as an example in Tab. 5. The limits for the combined fit are summarised in Tab. 6. To determine the limit on the mass of an excited electron M_{e^*} a fit is performed using $\left(\frac{d\sigma}{d\Omega}\right)_{\mathrm{e}^*}$ (Eq. 6). For the results given in Tab. 5 the coupling constant κ

			Fit result	
Model	λ	$\sqrt{s}$ [GeV]	λ	ϵ
$\left(\frac{d\sigma}{d\Omega}\right)_{\Lambda_\pm}$	$\pm 1/\Lambda_\pm^4$	130	$\left(4.3^{+20.6}_{-18.0}\right) \cdot 10^{-10}$ GeV^{-4}	0.999 ± 0.016
		136	$\left(7.1^{+19.3}_{-16.7}\right) \cdot 10^{-10}$ GeV^{-4}	0.999 ± 0.016
		161	$\left(1.53^{+5.12}_{-4.70}\right) \cdot 10^{-10}$ GeV^{-4}	1.001 ± 0.016
		172	$\left(-0.36^{+4.13}_{-3.76}\right) \cdot 10^{-10}$ GeV^{-4}	1.000 ± 0.016
		130 - 172	$\left(0.74^{+3.17}_{-2.97}\right) \cdot 10^{-10}$ GeV^{-4}	1.000 ± 0.016
$\left(\frac{d\sigma}{d\Omega}\right)_{\mathrm{QED}+7}$	$\lvert 1/\Lambda^6 \rvert$	130 - 172	$\left(5.57^{+35.9}_{-47.0}\right) \cdot 10^{-18}$ GeV^{-6}	1.000 ± 0.016
$\left(\frac{d\sigma}{d\Omega}\right)_{\mathrm{e}^*}$	$\lvert 1/M_{\mathrm{e}^*}^2 \rvert$	130 - 172	$\left(8.4^{+11.0}_{-27.9}\right) \cdot 10^{-6}$ GeV^{-2}	1.000 ± 0.016

Table 5: Results for fit parameters λ and ϵ. For $\Lambda_\pm$ the results for all energies are shown seperately. The error on the normalisation ϵ refects the assumed systematic error.

for the ($e^*e\gamma$)-vertex is fixed at $\kappa = 1$. Fig. 8 shows the upper limit (95 % CL) on κ^2 versus the mass of an excited electron M_{e^*}.

The angular distributions for all energies agree well with the QED expectation. The lower limits obtained from the combined fit on $\Lambda_\pm$, Λ and M_{e^*} are higher than existing published results using lower energies (see Ref. [18], [19], [20] and [21]) and are in agreement with other results obtained at this centre-of-mass energy [22]. Previous limits on the excited electron mass with $\kappa = 1$ are $M_{e^*} > 129$ GeV [21], 136 GeV [20] and 147 GeV [1].

A resonance X produced in the process $e^+e^- \to X\gamma$ and decaying photonically $X \to \gamma\gamma$ would be seen in the two photon invariant mass spectrum since this process leads to a three-photon final state without missing energy. This search has been performed previously at the Z^0-peak [23] and at higher energies [21]. The invariant mass of each photon pair is shown in Fig. 9 for all events of classes *II* and *III*. There are three entries for events with three clusters. Since the angular resolution is very precise, the energies of the three photons are calculated from the angles assuming three photon kinematics:

$$E_k \propto \sin\alpha_{ij} \; ; \; E_1 + E_2 + E_3 = \sqrt{s}, \tag{20}$$

with E_k the energy of one photon and α_{ij} the angle between the two other photons. For class *II* events $|\cos\theta| = 1$ is assumed for the unobserved photon. A typical mass resolution for photon pairs of about 0.5 (0.7) GeV can be achieved for class *III* (*II*). The distribution agrees well with the Monte Carlo expectation from the QED process $e^+e^- \to \gamma\gamma(\gamma)$, with no enhancement due to a resonance is observed. From the class *III* distribution an upper limit on the total production cross-section times the photonic branching ratio of an isotropically produced resonance is calculated using the method of Bock [24]. Combining the data of all centre-of-mass energies and subtracting the $e^+e^- \to \gamma\gamma(\gamma)$ background the limits shown in Fig. 10 are obtained. The mass range is defined by the phase space of the selection and limited due to the acollinearity restriction.

Parameter	Λ_+	Λ_-	Λ_6	Λ_7	Λ_8	M_{e^*}
[GeV]	195	210	793	483	15.5	194

Table 6: Summary of 95% CL lower limits obtained from the combined fit to the $\sqrt{s} = 130$, 136, 161 and 172 GeV angular distributions. The results are for the cut-off parameters $\Lambda_\pm$ and mass scales Λ according to QED+6, QED+7 and QED+8 expectation (Eqs. 3 - 5). Λ_6 and Λ_8 are derived from Λ_+ and Λ_7 respectively. The lower limit for the mass of an excited electron is also determined with the coupling constant κ assumed to be $\kappa = 1$.

8 Conclusions

The QED process $e^+e^- \to \gamma\gamma(\gamma)$ has been studied using data taken with the OPAL detector at LEP energies above the Z^0 resonance. Both the angular distributions and the total cross-section measurement agree well with QED predictions. Limits are set on cut-off parameters, mass scales for contact interactions ($\gamma\gamma e^+e^-$) and for non-standard γe^+e^- couplings, as well

as on the mass of an excited electron coupling to eγ. These limits are listed in Tab. 6. In the $\gamma\gamma$ invariant mass spectrum of events with three final state photons, no evidence is found for a resonance X decaying to $\gamma\gamma$. No photonic event with four or more detected photons is observed.

9 Acknowledgements

We particularly wish to thank the SL Division for the efficient operation of the LEP accelerator at all energies and for their continuing close cooperation with our experimental group. We thank our colleagues from CEA, DAPNIA/SPP, CE-Saclay for their efforts over the years on the time-of-flight and trigger systems which we continue to use. In addition to the support staff at our own institutions we are pleased to acknowledge the
Department of Energy, USA,
National Science Foundation, USA,
Particle Physics and Astronomy Research Council, UK,
Natural Sciences and Engineering Research Council, Canada,
Israel Science Foundation, administered by the Israel Academy of Science and Humanities,
Minerva Gesellschaft,
Benoziyo Center for High Energy Physics,
Japanese Ministry of Education, Science and Culture (the Monbusho) and a grant under the Monbusho International Science Research Program,
German Israeli Bi-national Science Foundation (GIF),
Bundesministerium für Bildung, Wissenschaft, Forschung und Technologie, Germany,
National Research Council of Canada,
Hungarian Foundation for Scientific Research, OTKA T-016660, T023793 and OTKA F-023259.

References

[1] OPAL Collaboration, G. Alexander et al., Phys. Lett. **B377** (1996) 222

[2] OPAL Collaboration, K. Ackerstaff et al., Phys. Lett. **B391** (1997) 210

[3] OPAL Collaboration, K. Ahmet et al., Nucl. Instr. and Meth. **A305** (1991) 275

[4] F.A. Berends and R. Kleiss, Nucl. Phys. **B186** (1981) 22

[5] S. Jadach et al., Phys. Lett. **390** (1997) 298

[6] D. Karlen, Nucl. Phys. **B289** (1987) 23

[7] G. Montagna et al., Nucl. Phys. **B452** (1996) 161

[8] S. Jadach et al., Comp. Phys. Comm. **66** (1991) 276

[9] T. Sjöstrand and M. Bengtsson, Comp. Phys. Comm. **43** (1987) 367
T. Sjöstrand, Comp. Phys. Comm. **39** (1986) 347

[10] OPAL Collaboration, J. Allison et al., Nucl. Instr. and Meth. **A317** (1992) 47

[11] I. Harris and L.M. Brown, Phys. Rev. **105** (1957) 1656
F.A. Berends and R. Gastmans, Nucl. Phys. **B61** (1973) 414

[12] S.D. Drell, Ann. Phys. **4** (1958) 75

[13] O.J.P. Éboli, A.A. Natale and S.F. Novaes, Phys. Lett. **B271** (1991) 274

[14] A. Litke, Ph.D.Thesis, Harvard University, unpublished (1970)

[15] G.D. Lafferty and T.R. Wyatt, Nucl. Instrum. Meth. **A355** (1995) 541

[16] MINUIT Reference Manual, F. James and M. Roos, CERN Program Library **D506**

[17] Review of Particle Physics, R.M. Barnett et al., Phys. Rev. **D54** (1996) 1

[18] PLUTO Collaboration, C. Berger et al., Phys. Lett. **B59** (1980) 87
JADE Collaboration, W. Bartel et al., Z. Phys. **C19** (1983) 197
MARKJ Collaboration, B. Adeva et al., Phys. Rev. Lett. **53** (1984) 134
TASSO Collaboration, M. Althoff et al., Z. Phys. **C26** (1984) 337
CELLO Collaboration, H.J. Behrend et al., Phys. Lett **B168** (1986) 420
HRS Collaboration, M. Derrick et al., Phys. Rev. **D34** (1986) 3286
MAC Collaboration, E. Fernandez et al., Phys Rev. **D35** (1987) 1
AMY Collaboration, H.J. Kim, et al., KEK preprint **89-52** (1989)
VENUS Collaboration, K. Abe et al., Z. Phys. **C45** (1989) 175
TOPAZ Collaboration, K. Shimozawa et al., Phys. Lett. **B284** (1992) 144
ALEPH Collaboration, D. Buskulic et al., Z. Phys. **C59** (1993) 215
DELPHI Collaboration, P. Abreu et al., Phys. Lett. **B268** (1991) 296
L3 Collaboration, O. Adriani et al., Phys. Lett. **B288** (1992) 404

[19] OPAL Collaboration, M.Z. Akrawy et al., Phys. Lett **B257** (1991) 531

[20] ALEPH Collaboration, D. Buskulic et al., Phys. Lett. **B384** (1996) 333

[21] L3 Collaboration, M. Acciarri et al., Phys. Lett. **B384** (1996) 323

[22] L3 Collaboration, M. Acciarri et al., CERN-PPE/97-77, submitted to Phys. Lett.

[23] OPAL Collaboration, P.D. Acton et al., Phys. Lett **B311** (1993) 391
L3 Collaboration, M. Acciarri et al., Phys. Lett. **B345** (1995) 609

[24] P. Bock, *Determination of Exclusion Limits for Particle Production Using Different Decay Channels with Different Energies, Mass Resolutions and Backgrounds*, submitted to Nucl. Instrum. Meth. (1997)

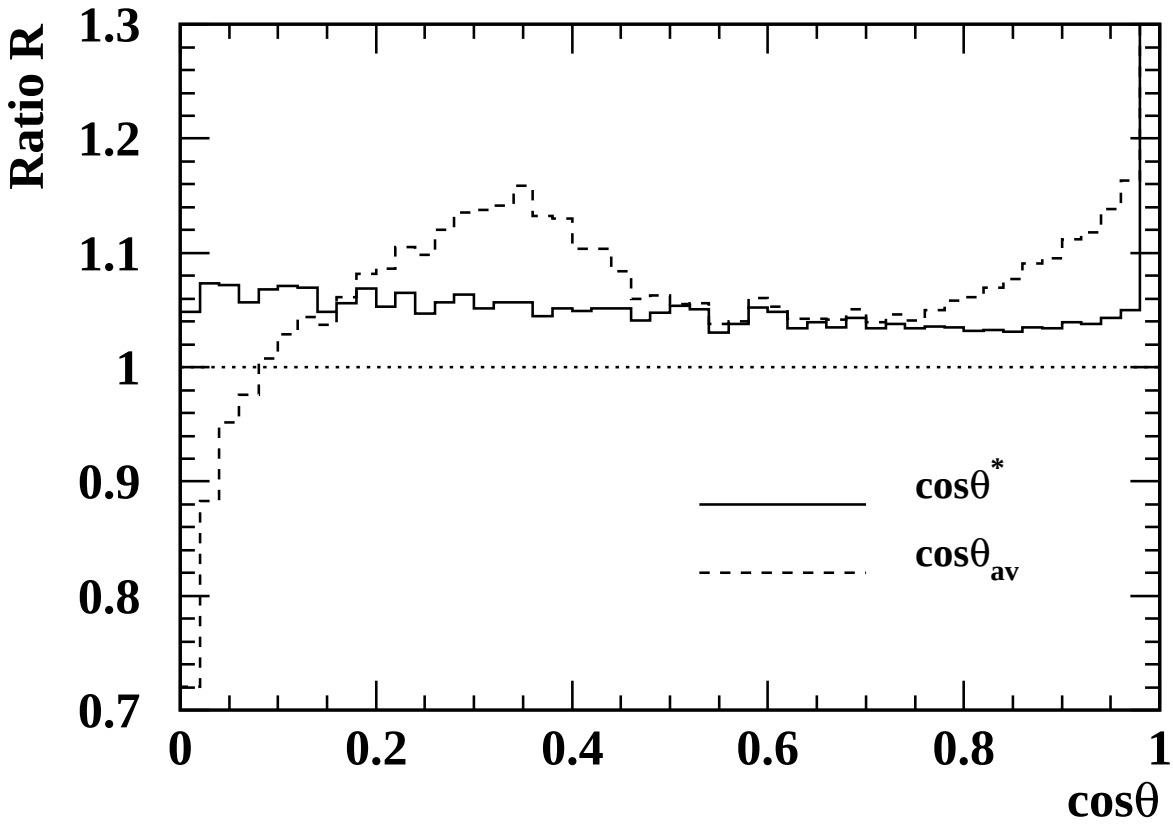

Figure 1: Ratio of the differential cross-section for the $e^+e^- \to \gamma\gamma(\gamma)$ Monte Carlo sample relative to the Born cross-section, $\mathcal{R} = \left(\frac{d\sigma}{d\Omega}\right)_{\rm MC} / \left(\frac{d\sigma}{d\Omega}\right)_{\rm Born}$. $\mathcal{R}$ is shown here for both angular definitions $\cos\theta_{\rm av}$ (Eq. 7) and $\cos\theta^*$ (Eq. 8). The event angle is calculated from the two photons with the highest generated energy.

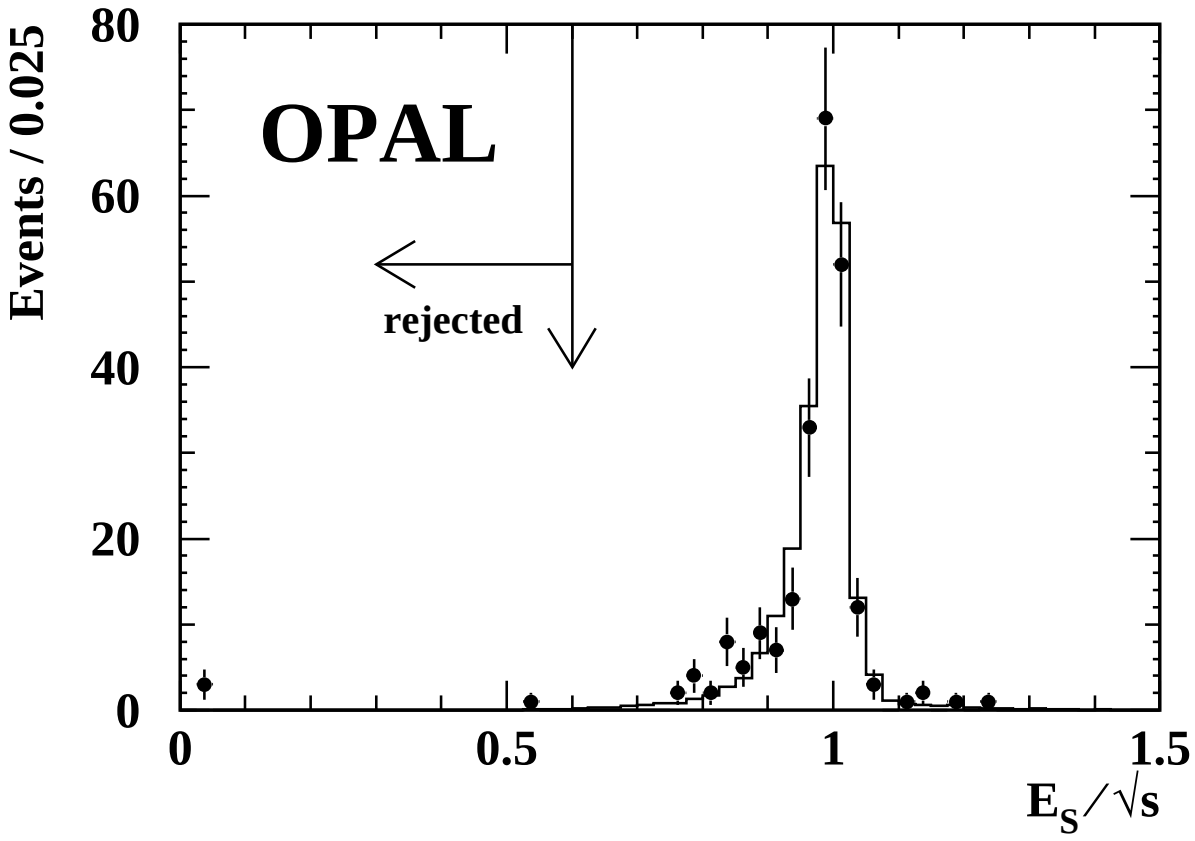

Figure 2: Scaled sum of the two highest cluster energies for all events with an acollinearity angle $\zeta < 10^\circ$ (corresponding to class I). The points with error bars represent the data, the histogram the $e^+e^- \to \gamma\gamma(\gamma)$ Monte Carlo expectation. The cut on this quantity is indicated.

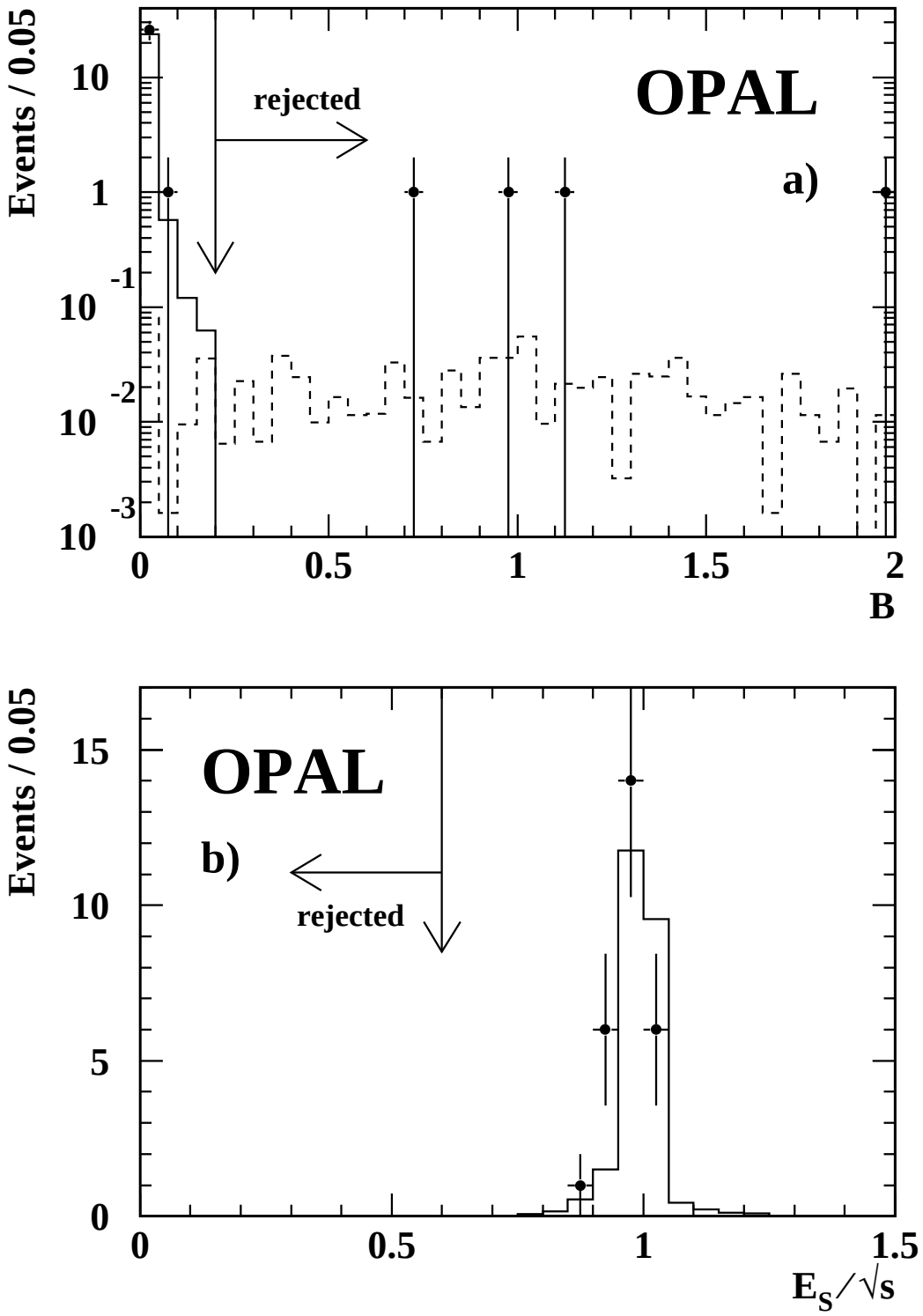

Figure 3: Event distributions for data in class *II* for $\sqrt{s}$ = 130, 136, 161 and 172 GeV. Plot a) shows the distribution of the imbalance $\mathcal{B}$, a measure of the scaled transverse momentum (for definition see Eq. 11) together with the selection cut. Plot b) shows the scaled sum of both cluster energies plus E_{lost} after the cut on $\mathcal{B}$. The cut is indicated. The points represent the data, the solid histogram the Monte Carlo expectation from $e^+e^- \to \gamma\gamma(\gamma)$ and the dashed histogram the Monte Carlos expectation from background (mainly $\nu\overline{\nu}\gamma\gamma$).

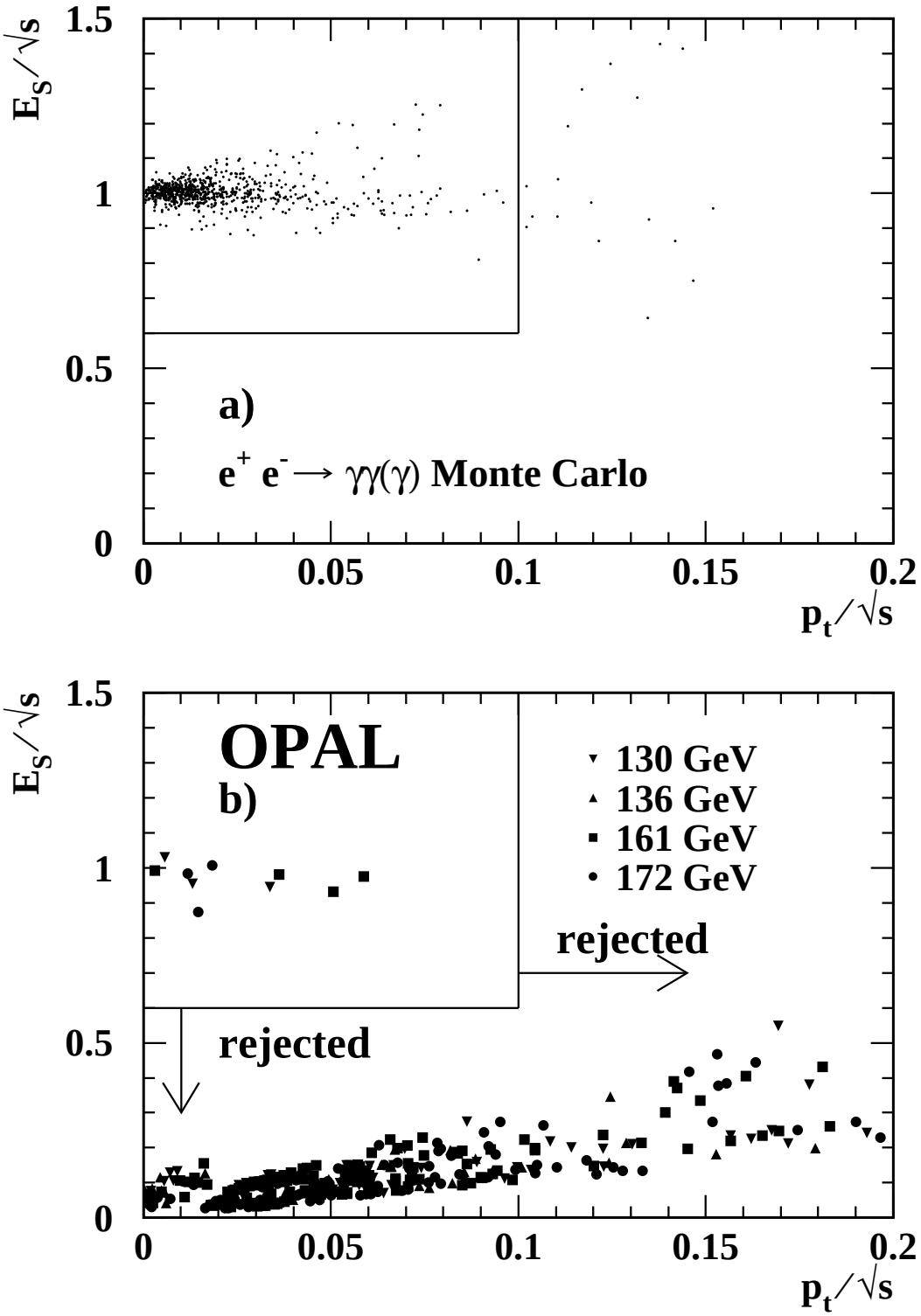

Figure 4: The scaled energy sum versus the scaled transverse momentum for class *III* events, for a) $e^+e^- \rightarrow \gamma\gamma(\gamma)$ Monte Carlo and b) the OPAL data. The box indicates the selected region. The background comes mainly from cosmic ray events.

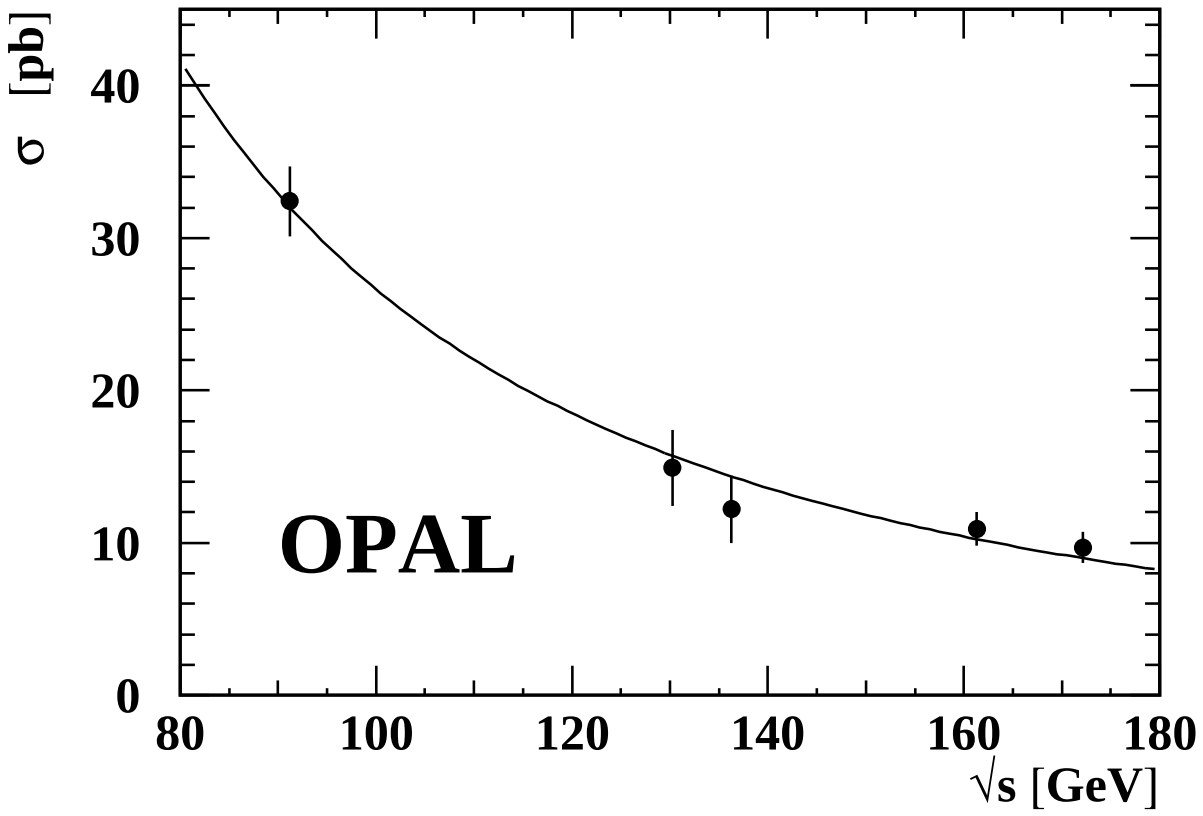

Figure 5: Total cross-section for the process $e^+e^- \to \gamma\gamma$ with $\cos\theta < 0.9$. The data are corrected for efficiency loss and higher order effects and correspond to a Born level measurement. The result at the Z^0 is taken from Ref. [19]. The curve corresponds to the Born level QED prediction.

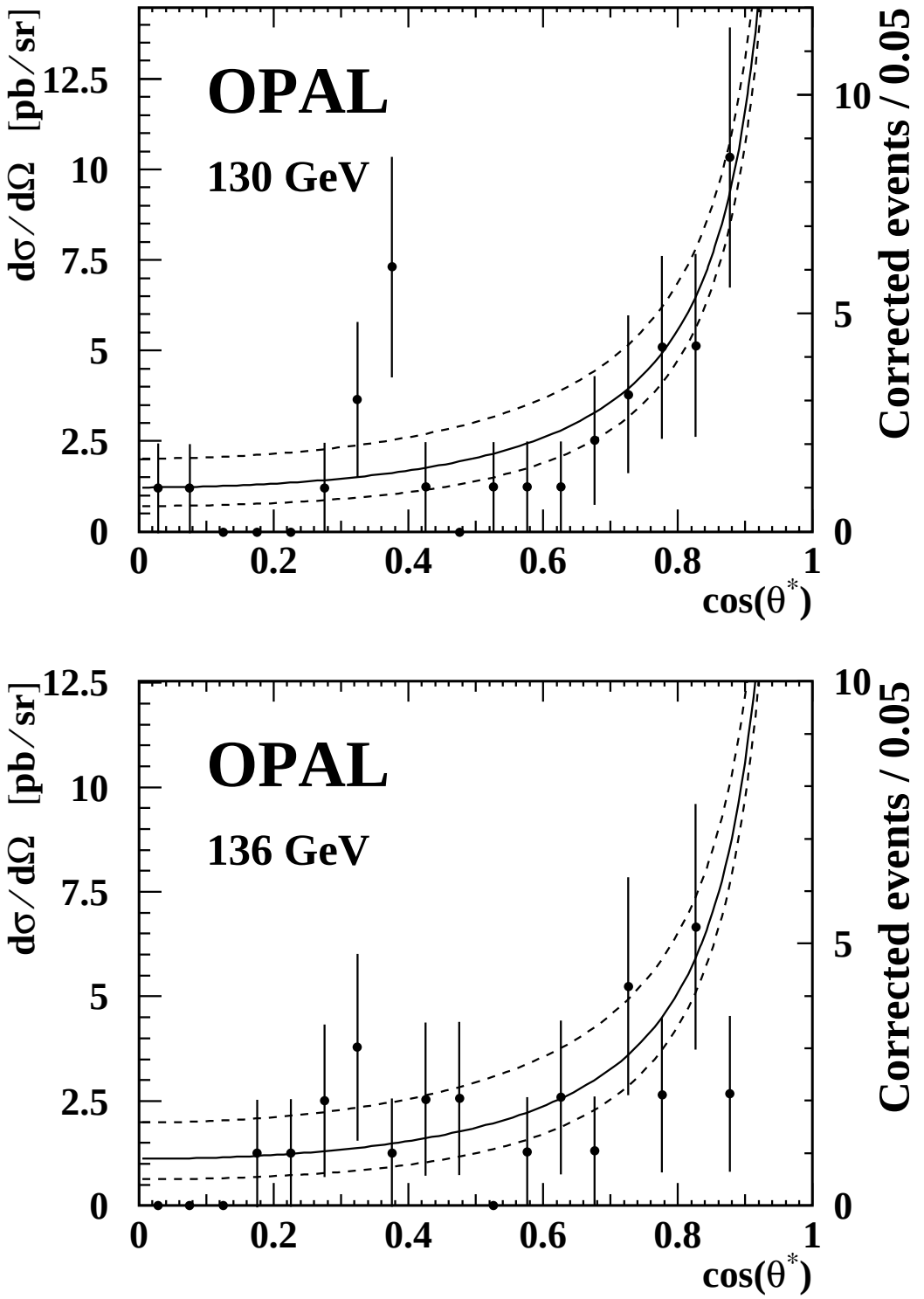

Figure 6: The measured angular distribution for the process $e^+e^- \to \gamma\gamma(\gamma)$ as selected in the three classes at $\sqrt{s} = 130$ and 136 GeV. The data points show the efficiency-corrected number of events; radiative corrections are also included. The solid curve corresponds to the Born level QED prediction. The dotted lines represent 95% CL intervals of the fit to the function $\left(\frac{d\sigma}{d\Omega}\right)_{\Lambda_\pm}$.

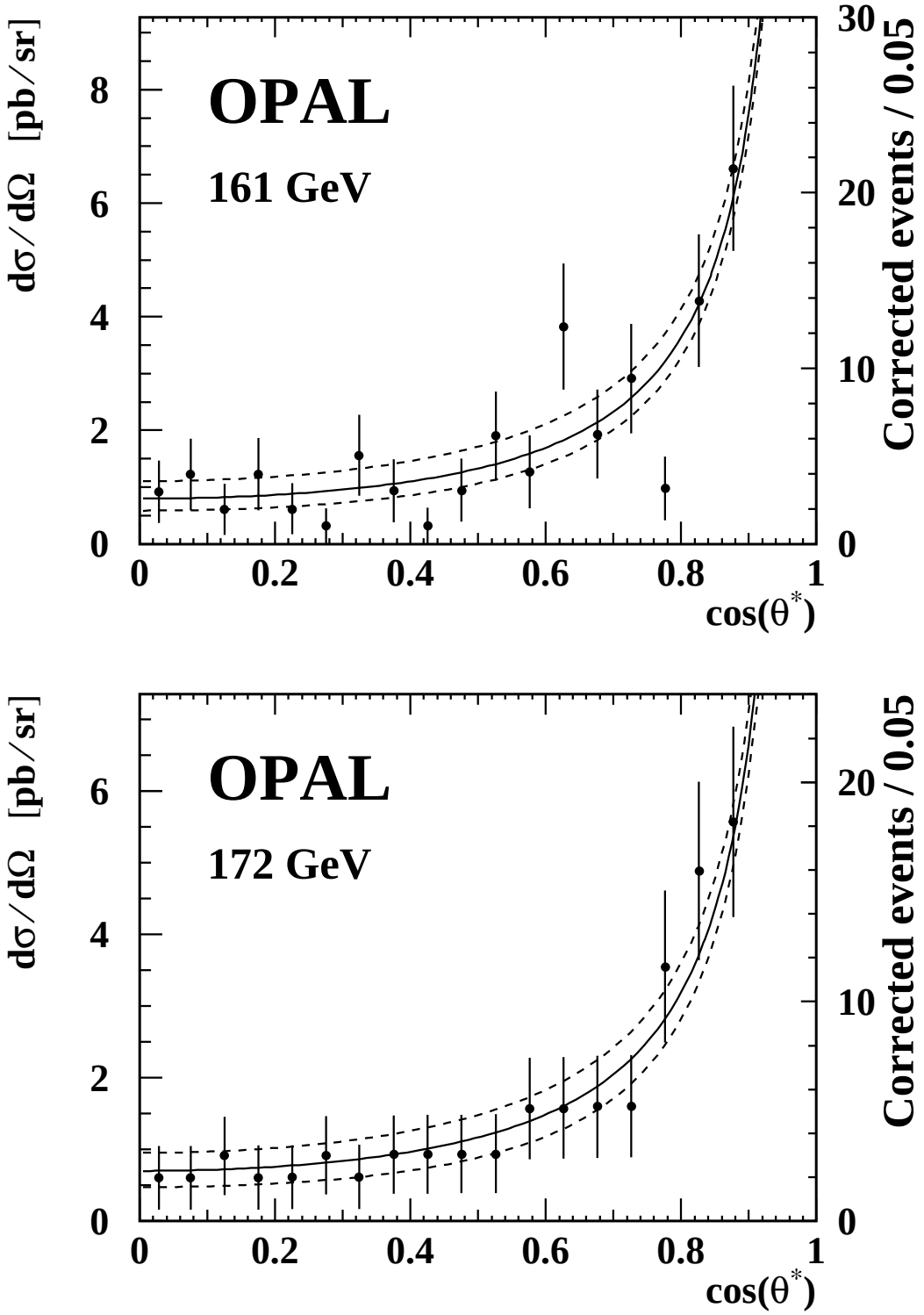

Figure 7: The measured angular distribution for the process $e^+e^- \to \gamma\gamma(\gamma)$ as selected in the three classes at $\sqrt{s} = 161$ and 172 GeV. The data points show the efficiency-corrected number of events; radiative corrections are also included. The solid curve corresponds to the Born level QED prediction. The dotted lines represent 95% CL intervals of the fit to the function $\left(\frac{d\sigma}{d\Omega}\right)_{\Lambda_\pm}$.

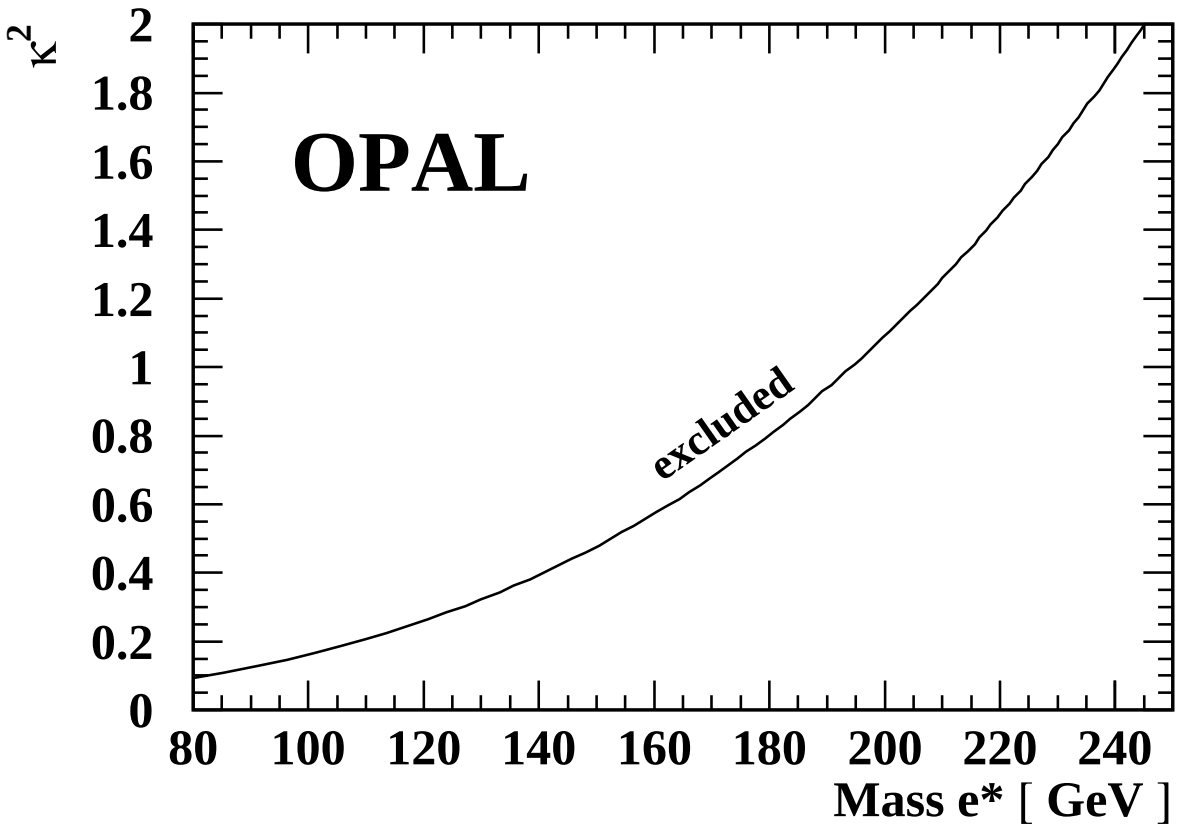

Figure 8: Upper limit (95 % CL) on the square of the coupling constant κ^2 as a function of the mass of an excited electron M_{e^*}.

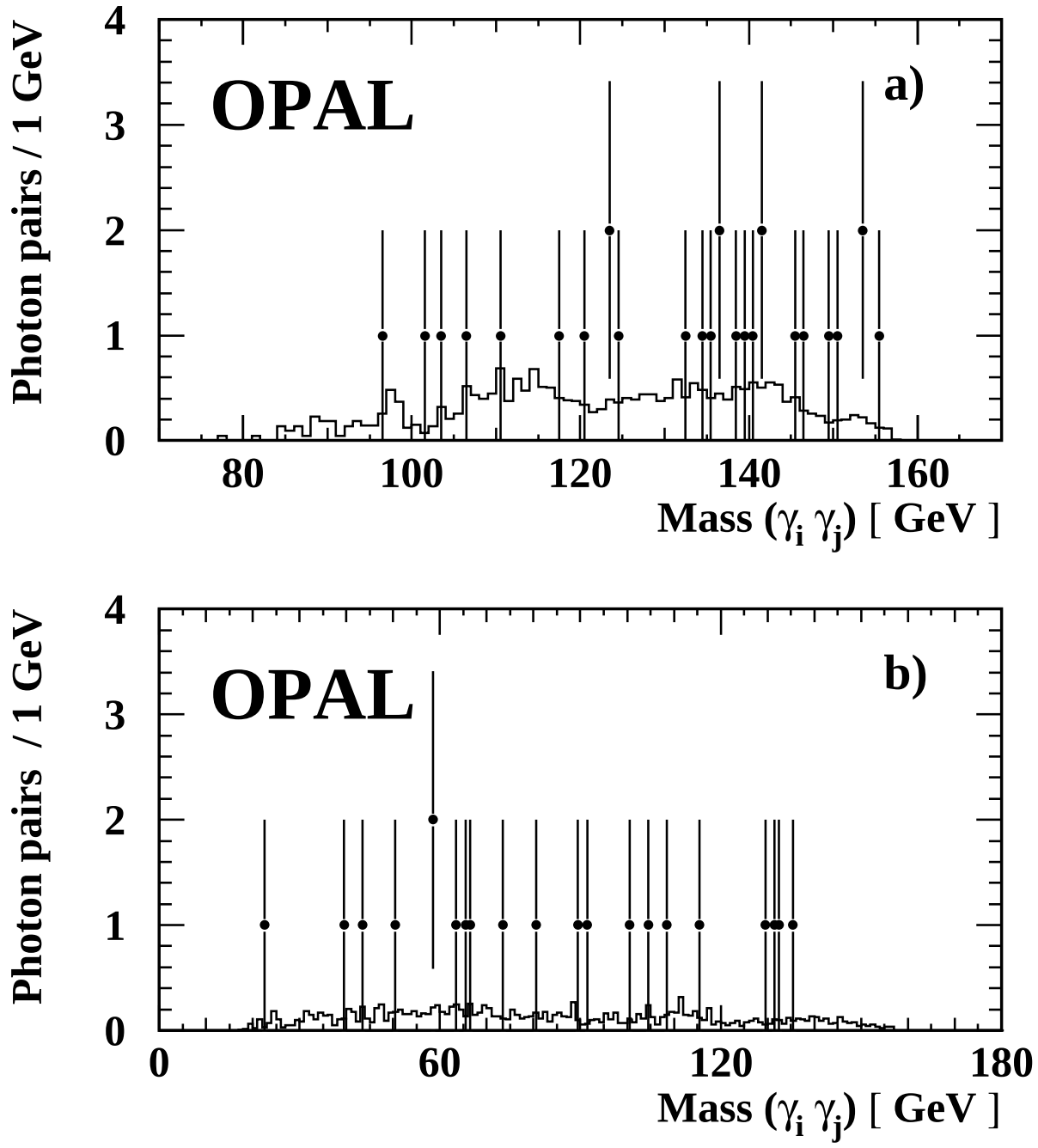

Figure 9: The invariant mass of photon pairs for a) class *II* events and b) class *III* events. The points are the data, the histogram the $e^+e^- \to \gamma\gamma(\gamma)$ Monte Carlo expectation. There is one entry per event for class *II* events and three entries per event for class *III* events.

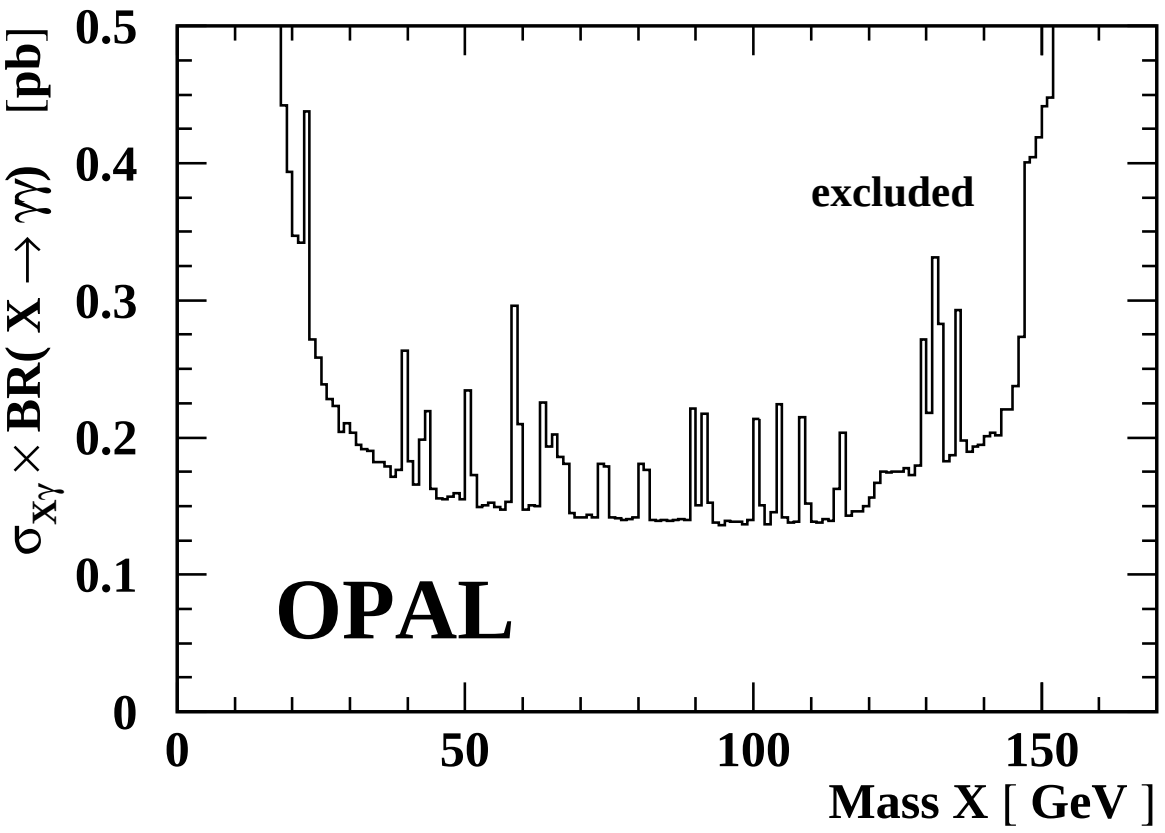

Figure 10: Lower limits (95 % CL) for the cross section times branching ratio for the process $e^+e^- \to X\gamma$, $X \to \gamma\gamma$ as a function of the mass of the resonance X. The $e^+e^- \to \gamma\gamma(\gamma)$ background is subtracted. The step at 120 GeV comes from the phase space limit of the 130 and 136 GeV data.